Journal of Magnetism and Magnetic Materials 422 (2017) 93–99

Contents lists available at ScienceDirect

Journal of Magnetism and Magnetic Materials

journal homepage: www.elsevier.com/locate/jmmm

X-ray magnetic circular dichroism study of Dy-doped Bi_2Te_3 topological insulator thin films

A.I. Figueroa [a], A.A. Baker [a,b], S.E. Harrison [b,c], K. Kummer [d], G. van der Laan [a], T. Hesjedal [b,*]

[a] Magnetic Spectroscopy Group, Diamond Light Source, Didcot, OX11 0DE UK
[b] Department of Physics, Clarendon Laboratory, University of Oxford, Oxford, OX1 3PU UK
[c] Department of Electrical Engineering, Stanford University, Stanford, CA, 94305 USA
[d] European Synchrotron Radiation Facility, BP 220, Grenoble Cedex, F-38043 France

ARTICLE INFO

Article history:
Received 27 January 2016
Received in revised form
8 August 2016
Accepted 21 August 2016
Available online 24 August 2016

Keywords:
Topological insulators
Magnetic doping
Magnetic spectroscopy
XMCD
Molecular beam epitaxy

ABSTRACT

Magnetic doping of topological insulators (TIs) is crucial for unlocking novel quantum phenomena, paving the way for spintronics applications. Recently, we have shown that doping with rare earth ions introduces large magnetic moments and allows for high doping concentrations without the loss of crystal quality, however no long range magnetic order was observed. In Dy-doped Bi_2Te_3 we found a band gap opening above a critical doping concentration, despite the paramagnetic bulk behavior. Here, we present a surface-sensitive x-ray magnetic circular dichroism (XMCD) study of an *in situ* cleaved film in the cleanest possible environment. The Dy $M_{4,5}$ absorption spectra measured with circularly polarized x-rays are fitted using multiplet calculations to obtain the effective magnetic moment. Arrott–Noakes plots, measured by the Dy M_5 XMCD as a function of field at low temperatures, give a negative transition temperature. The evaporation of a ferromagnetic Co thin film did not introduce ferromagnetic ordering of the Dy dopants either; instead a lowering of the transition temperature was observed, pointing towards an antiferromagnetic ordering scenario. This result shows that there is a competition between the magnetic exchange interaction and the Zeeman interaction. The latter favors the Co and Dy magnetic moments to be both aligned along the direction of the applied magnetic field, while the exchange interaction is minimized if the Dy and Co atoms are antiferromagnetically coupled, as in zero applied field.

1. Introduction

Magnetic doping of topological insulators (TIs) [1], resulting in the breaking of time-reversal symmetry (TRS), is crucial for unlocking novel quantum phenomena [2]. In three-dimensional TIs, the topological surface state (TSS) is protected by TRS, and magnetic doping leading to long-range ferromagnetic order with out-of-plane anisotropy is one possibility to open a gap in the TSS [3]. Such a magnetically induced band gap was first experimentally confirmed in Mn-doped Bi_2Se_3 using angle-resolved photoemission electron spectroscopy (ARPES) [4]. Long-range ferromagnetic ordering was induced in the prototypical 3D-TIs Bi_2Se_3 and Bi_2Te_3 upon Mn [5,6] and Cr doping [7–9].

Recently, we have shown that doping Bi_2Te_3 thin films with rare-earth (RE) ions, such as Gd, Ho, or Dy, introduces large magnetic moments and allows for high doping concentrations, however, no long-range magnetic order was observed [10–13]. In Dy-doped Bi_2Te_3 we found a band gap opening above a critical doping concentration using ARPES [14], persisting up to a temperature of 300 K, despite the paramagnetic bulk behavior [13]. However, the question of the origin of this band gap remains unanswered.

Despite the paramagnetic bulk behavior of Dy-doped films, there is the possibility of surface ferromagnetic ordering via the Ruderman–Kittel–Kasuya–Yosida (RKKY) interaction between the localized Dy moments and the TSS [1,3,15,16]. However, recent reports have also shown different scenarios, e.g., a band gap arising from magnetic surface clusters in the case of Cr-doped Bi_2Se_3 [17], or hybridization causing a temperature-independent gap of ~100 meV in Mn-doped Bi_2Se_3 [18]. As the intricate details of the interplay between the competing magnetic interactions depend critically on the chemical potential of the material [19], only surface-sensitive experiments on ultra-clean surfaces can determine the effective magnetic order in a given materials system.

Here, we present a surface-sensitive x-ray magnetic circular dichroism (XMCD) study of the structural and magnetic properties of an *in situ* cleaved film of Dy-doped Bi_2Te_3 in the cleanest possible UHV environment [20]. The magnetic order is investigated using the Arrott–Noakes criterion, which yields an estimate of the

* Corresponding author.
E-mail address: Thorsten.Hesjedal@physics.ox.ac.uk (T. Hesjedal).

http://dx.doi.org/10.1016/j.jmmm.2016.08.063

critical temperature of the sample. No ferromagnetic ordering was found at the surface of a cleaved sample, which is identical to the one that showed a gap opening in ARPES [14]. Next, we attempted to introduce ferromagnetic order via proximity-coupling of Co adatoms. Instead of finding increased ordering, we measured a decrease of the critical temperature of the Dy-doped sample [21], which may be due to antiferromagnetic alignment between the Dy and Co atoms at the interface.

2. Sample fabrication and magnetic properties

$(Dy_xBi_{1-x})_2Te_3$ thin films, with x denoting the substitutional Dy concentration, were grown by molecular beam epitaxy (MBE) on c-plane sapphire substrates [13]. The rhombohedral films were prepared using a two-step growth recipe with a final substrate temperature of 300 °C. The films are free of secondary phases as confirmed by x-ray diffraction and transmission electron microscopy [14]. The growth recipe and the structural properties of the films are described in detail in Refs. [13,14]. The films investigated in this study have a Dy concentration of $x=0.055$ and 0.113. For the lower concentration the TSS band structure remains intact and shows a linear dispersion, whereas for the higher concentration a sizeable gap was observed in ARPES [14], suggesting a possible change in magnetic properties.

The bulk magnetic properties of $(Dy_xBi_{1-x})_2Te_3$ thin films was measured using a superconducting quantum interference device (SQUID) magnetometer with the field applied in-plane; the data is shown in Ref. [13]. No hysteretic behavior is observed. As discussed in detail in Ref. [13], the saturation magnetization of Dy-doped samples is doping concentration-dependent—much different from Gd- and Ho-doped Bi_2Te_3 samples [11,12]. The inverse susceptibility $1/\chi = H/M$ of the samples can be fitted by a straight line, as expected from a paramagnetic system following the Curie–Weiss law.

3. X-ray spectroscopy

3.1. Experimental

X-ray absorption spectroscopy (XAS) and XMCD measurements were performed on beamline I10 at the Diamond Light Source, UK, and beamline ID32 at the European Synchrotron Radiation Facility (ESRF), France. XAS was detected simultaneously in bulk-sensitive fluorescence yield (FY) and total-electron-yield (TEY) mode. TEY is surface sensitive giving a probing depth of ~4 nm at the Co $L_{2,3}$ edge [20], increasing to ~6 nm at the Dy $M_{4,5}$ edge [22]. The XMCD was obtained as the difference between two XAS spectra recorded with the helicity vector antiparallel and parallel to the applied magnetic field $(\mu^- - \mu^+)$, where μ is the absorption coefficient. Measurements were performed with the x-ray beam, which is parallel to the applied magnetic field, impinging at 20° grazing incidence on the sample.

XAS and XMCD measurements were performed on the $(Dy_xBi_{1-x})_2Te_3$ samples after *in situ* cleaving in the UHV environment ($\lesssim 10^{-9}$ Torr) of the superconducting magnet chamber. The XAS and XMCD spectra for the $x=0.055$ sample are shown in Fig. 1 (a) and (b), respectively, measured in both TEY and FY mode. The maximum of the Dy M_5 edge is located at 1292.9 eV photon energy [22]. There are considerable differences in line shape between the TEY and FY spectra that are not due to saturation and self-absorption effects, which are small for low concentrations. A comparison for the Dy M_5 XMCD shows that the positive peak at ~1289 eV is smaller, but the negative peak at ~1293 eV is larger in

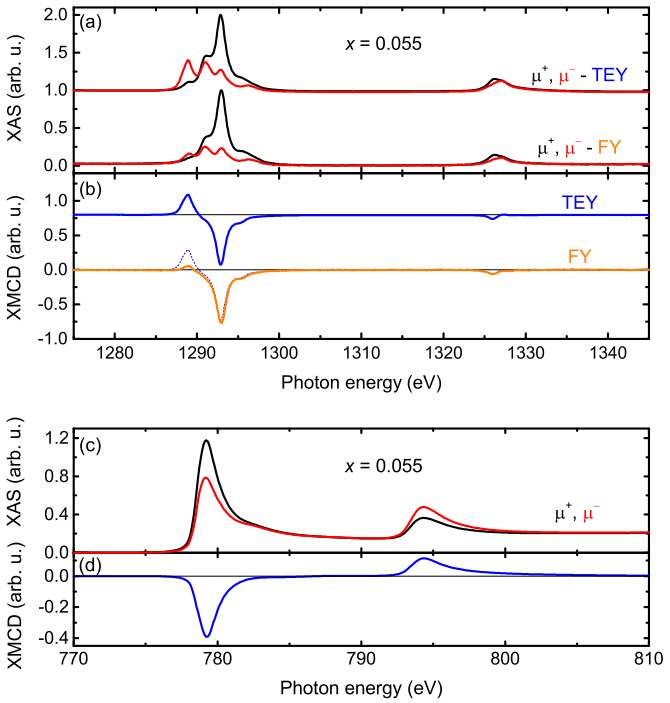

Fig. 1. (a,b) Dy $M_{4,5}$ spectra of *in situ* cleaved $(Dy_xBi_{1-x})_2Te_3$ ($x=0.055$) thin film. (a) XAS spectra for opposite circular polarization (μ^+, μ^-) measured in TEY and FY detection modes. (b) Corresponding XMCD spectra $(\mu^- - \mu^+)$ in TEY and FY mode. Spectra have been offset for clarity. The TEY XMCD (thin dashed line) is also overlaid on the FY to permit a quantitative comparison. (c,d) Co $L_{2,3}$ spectra of an *in situ* deposited 3-nm-thick Co layer grown on top of the cleaved $x=0.055$ film, measured in TEY mode at 10 K in remanence after ramping the field up to 1 T. (c) XAS and (d) XMCD spectra. The clean, metallic line shape indicates that no significant intermixing or alloying has occurred.

FY than in TEY. This behavior is in agreement with the multiplet spectra calculated by van Veenendaal and Benoist [23]. The reason for the discrepancy is that, in contrast to the TEY, the FY is not proportional to the absorption cross-section because it also depends on the decay rate. The latter varies with the intermediate (XAS) state, where states at higher photon energies normally have higher fluorescence decay rates [20].

Ferromagnetic Co was evaporated onto the pristine surface of the $x=0.055$ sample, with the goal of introducing or enhancing the ferromagnetic order through proximity coupling [21], using an electron beam-evaporator mounted in the XAS measurement chamber. The sample was kept at 10 K during this process to inhibit reactions between the incident Co atoms and the clean sample surface [24]. The base pressure during evaporation was $<1\times10^{-9}$ Torr. The XMCD measurements were performed in regular intervals during the deposition to check lineshape and remanent magnetization. This way, the final thickness of the Co layer was determined to be ~3 nm. Fig. 1(c) and (d) shows the XAS and XMCD for the thin Co layer deposited onto the cleaved sample. The spectra show no evidence of alloying between Co and the underlying sample.

The magnetic proximity effect in the Dy-doped TI is measured using the surface sensitive TEY signal, which only probes the region close to the Co capping.

3.2. Calculated spectra

Electric-dipole transitions from the $3d$ core level in REs are allowed to empty $4f$ states, but forbidden to $5d$ and $6s$ valence states. For the multi-electronic configuration of the Dy^{3+}, the $4f^9 \rightarrow 3d^9 4f^{10}$ transitions can be calculated using atomic multiplet

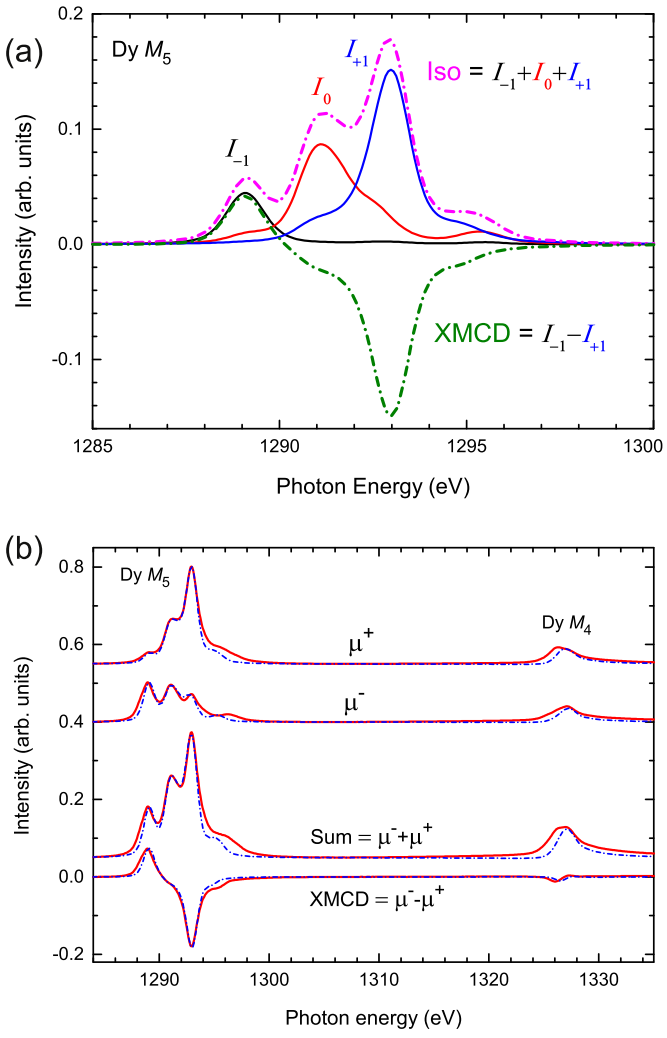

Fig. 2. XAS and XMCD spectra at the Dy $M_{4,5}$ edges. (a) Calculated XAS for left circular (I_{-1}), right circular (I_{+1}), and linear polarization along magnetization direction (I_0), together with the isotropic spectrum ($I_{-1}+I_0+I_{+1}$) and XMCD spectrum ($I_{-1}-I_{+1}$). (b) Experimental μ^+ and μ^- spectra (solid red lines) of the cleaved sample with $x=0.055$ at 7 T and 6.2 K at grazing incidence, and their sum and difference spectra compared with the calculated spectra (dash-dotted blue lines). The experimental spectra were fitted with the calculated spectra I_{-1}, I_0, and I_{+1} from (a), yielding the relative intensity ratios given in Eq. (1). Spectra have been offset for clarity. (For interpretation of the references to color in this figure caption, the reader is referred to the web version of this paper.)

theory, in which spin–orbit and electrostatic interactions are treated on an equal footing [22,25]. The intra-atomic electrostatic interactions include the 3*d*–4*f* and 4*f*–4*f* Coulomb and exchange interactions. The wave functions of the initial- and final-state configurations are calculated in intermediate coupling using Cowan's atomic Hartree–Fock code with relativistic corrections [25–27].

Following the standard procedure to account for interatomic interactions [22], the parameters of the Slater integrals for the Coulomb and exchange interactions were reduced to 65%, while the spin–orbit interaction was kept at 100%. The Dy M_5 (M_4) line spectra were convoluted by a Lorentzian of $\Gamma=0.25$ eV (0.5 eV) for intrinsic lifetime broadening and a Gaussian of $\sigma=0.35$ eV for instrumental broadening. The intrinsic lifetime at the M_4 is broader than at the M_5 edge due to Coster–Kronig decay [22].

The calculated spectra I_q are shown in Fig. 2(a) for parallel ($q=+1$) and antiparallel ($q=-1$) alignment of the x-ray helicity vector and applied magnetic field, and for linear polarization along the magnetization direction ($q=0$). Also shown are the isotropic spectrum ($I_{-1}+I_0+I_{+1}$) and XMCD ($I_{-1}-I_{+1}$); for sign convention see Ref. [20].

Sum rules relate the integrated intensities of the XAS and XMCD $M_{4,5}$ spectra to the ground state expectation values of the orbital and spin moments [28,29], and were used for the $L_{2,3}$ edges of Mn, Fe, and Co dopants and adatoms in TIs [9,24].

For the REs the sum rule analysis is less straightforward [30] because of (i) the large *jj* mixing between the $3d_{5/2}$ and $3d_{3/2}$, which requires a correction factor, (ii) the linear dichroism, which has to be taken into account in the sum spectra for the normalization per hole, and (iii) the presence of a usually large magnetic dipole term T_z.

Under the condition that the 4*f* crystalline electrostatic field is small compared to the 4*f* spin–orbit interaction, the spin and orbital moments remain parallel, so that their ratio is fixed [31]. Then, as a function of the magnetization, *M*, the XMCD intensity scales with *M*, while the isotropic intensity remains constant. Thus the scaling factor for the magnetic moment is directly obtained from the reduction in the asymmetry $(\mu^- - \mu^+)/(\mu^- + \mu^+)$ compared to the theoretical value $(I_{-1}-I_{+1})/I_{-1}+I_{+1})$. This method has been used in Refs. [6,11].

Here, we will employ an alternative method to determine the magnetic moments. This method is based on the fact that for most heavy REs the multiplet structure has distinct peaks that can be assigned to left- and right-circular polarization [22]. The Dy M_5 absorption structure is well suited to determine the relative contributions of the three fundamental spectra, I_{-1}, I_0, and I_{+1}, since their respective peaks are well separated in photon energy by ~2 eV each. Fig. 2(a) shows that the main peak at 1292.9 eV is almost purely I_{+1} with only a few percent of I_0. Likewise, the low-energy peak is almost purely I_{-1}. On the other hand, the M_4 intensity is much lower and less suitable for polarization analysis. Nonetheless, also here the measured XAS and XMCD is in good agreement with the calculation [22,32].

The experimental Dy $M_{4,5}$ spectra, μ^- and μ^+, for the cleaved sample with $x=0.055$ at 7 T and 6.2 K at grazing incidence were fitted using the calculated I_{-1}, I_0, and I_{+1} spectra from Fig. 2(a). Results are shown in Fig. 2(b), where the fitting yields

$$\mu^- = 62.5\%I_{-1} + 29.5\%I_0 + 8.0\%I_{+1},$$
$$\mu^+ = 12.5\%I_{-1} + 32.3\%I_0 + 55.2\%I_{+1}, \quad (1)$$

which gives polarization scaling factors for the magnetic moment of 0.545 and 0.427, respectively. The polarization factor for μ^+ is lower due to the extra intensity in the experimental spectra around 1296 eV, which is less pronounced in the calculation. Since the μ^- spectrum shows no such deficiency, its result is more accurate. Hence we take the somewhat higher polarization factor for μ^-.

The *LS*-coupled Hund's rule ground state, Dy^{3+} $4f^9$ ($^6H_{15/2}$) with spin, orbital, and total magnetic moments, $S=5/2$, $L=5$, and $J=15/2$ gives a Landé splitting factor $g_J=4/3$ and an effective magnetic moment $\mu_{\text{eff}}=g_J\sqrt{J(J+1)}=10.65\,\mu_B$/Dy. Assuming that the x-ray beam is fully polarized, the μ^- spectrum gives a magnetic moment that is 54.5% of the Hund's rule ground state value. Hence, from the XMCD on our sample, we obtain an effective magnetic moment of $\mu_{\text{eff}}=5.8\,\mu_B$/Dy. SQUID magnetometry of this sample yielded a saturation magnetization of $\mu_{\text{eff}}\approx 8.3\,\mu_B$/Dy, which is also less than the free ion Hund's rule value. While the XMCD measures only the 4*f* moment on the Dy atoms, SQUID measures all moments including also the Dy 5*d* moment and any induced magnetization on the Te atoms.

These results show that the Dy atoms are far from completely magnetized. However, the observed dichroism is similar in size as was seen for other polarized Dy spectra in the literature [33–35]. We expect that the common cause of the reduced moment is the

presence of a small crystal field on the Dy 4*f* electrons. Crystal-field effects might play an important role in explaining the reduction of the effective magnetic moment observed for Dy dopants since the Dy atoms are substituting Bi in the Bi_2Te_3 lattice, which are in an octahedral environment of Te atoms. The importance of crystal field effects at low temperatures is well established in the literature, but difficult to quantify theoretically [36].

4. Arrott–Noakes analysis

In order to investigate the magnetic order on the surface of the pristine $(Dy_xBi_{1-x})_2Te_3$ thin film, the critical behavior was analyzed using the Arrott–Noakes plot criterion. This leads to an estimation of the critical temperature, T_C, of a transition from a non-magnetic to a magnetically ordered system. The criterion consists of plotting the isothermal variations of M^2 as a function of H/M, with M being the magnetization and H the applied field, which should yield straight lines according to [21,37]

$$M^2 = A(H/M) + B(T - T_C), \tag{2}$$

where T is the temperature, and A and B are constants. The intercept of the isotherms with the H/M axis, i.e., where $M^2 = 0$, is positive (negative) for $T > T_C$ ($T < T_C$), so that T_C is equal to that temperature for which the intercept is zero.

Arrott and Noakes [38] generalized this criterion to express the equation of state for a magnetic system near its critical temperature in terms of the critical exponents β and γ, as

$$M^{1/\beta} = C_1(T - T_C) + C_2(H/M)^{1/\gamma}, \tag{3}$$

where C_1 and C_2 are constants. In the long-range mean-field model, these exponents are $\beta = 0.5$ and $\gamma = 1$, which yields Eq. (2). In the nearest-neighbor 3D Heisenberg model, the corresponding values are $\beta = 0.36$ and $\gamma = 1.386$.

Fig. 3 shows M vs H, Arrott plots (i.e., M^2 vs H/M) and Arrott–Noakes plots (i.e., $\boldsymbol{M}^2$ vs $(H/M)^{1/\gamma}$) at various temperatures for the $(Dy_xBi_{1-x})_2Te_3$ thin film with $x=0.113$. We use the background-corrected Dy M_5 XMCD asymmetry, $(\mu^- - \mu^+)/(\mu^- + \mu^+)$, which is directly proportional to M at the Dy site. The top panel depicts surface-sensitive TEY measurements, while the lower panel shows results for bulk-sensitive FY. M^2 vs H/M curves (Fig. 3(b) and (e)) do not yield linear behavior, which indicates that the mean-field model does not appropriately describe this material. Instead, we applied the Arrott–Noakes criterion which uses the values of β and γ for the 3D Heisenberg model. These curves are shown in Fig. 3 (c) and (f). By fitting parallel straight lines to the high-field regions (forcing the gradient of all lines to the same value) we obtain the $(H/M)^{1/\gamma}$ intercepts, collected in Fig. 5(a). The zero points of these intercepts give $T_C = (-14 \pm 1)$ K and (-9 ± 2) K for the TEY and FY data, respectively.

Similarly, M vs H, Arrott, and Arrott–Noakes plots for the $x=0.055$ sample are shown in Fig. 4. A comparison of the $\boldsymbol{M}$ vs $\boldsymbol{H}$ plot obtained for the *as-cleaved* sample and that with the Co overlayer measured at 14 K is depicted in Fig. 4(a). The fact that the latter curve lies underneath the *as-cleaved* sample indicates a decrease in M, which, at the same time, suggests a decrease in T_C for the Dy atoms at the interface of the Dy-doped sample and the Co layer.

The full set of Arrott–Noakes plots, measured in TEY mode, for the $x=0.055$ sample with an Co overlayer are shown in Fig. 4(d). The $(H/M)^{1/\gamma}$-intercepts obtained from the linear fits of the high-field region of each isotherm are plotted in Fig. 5(b). T_C extracted from the zero point of the intercept yields a value of (-2.0 ± 0.8) K. Note that this value is greater than that found for the $x=0.113$ sample (-14 ± 1 K), but given the different Dy doping

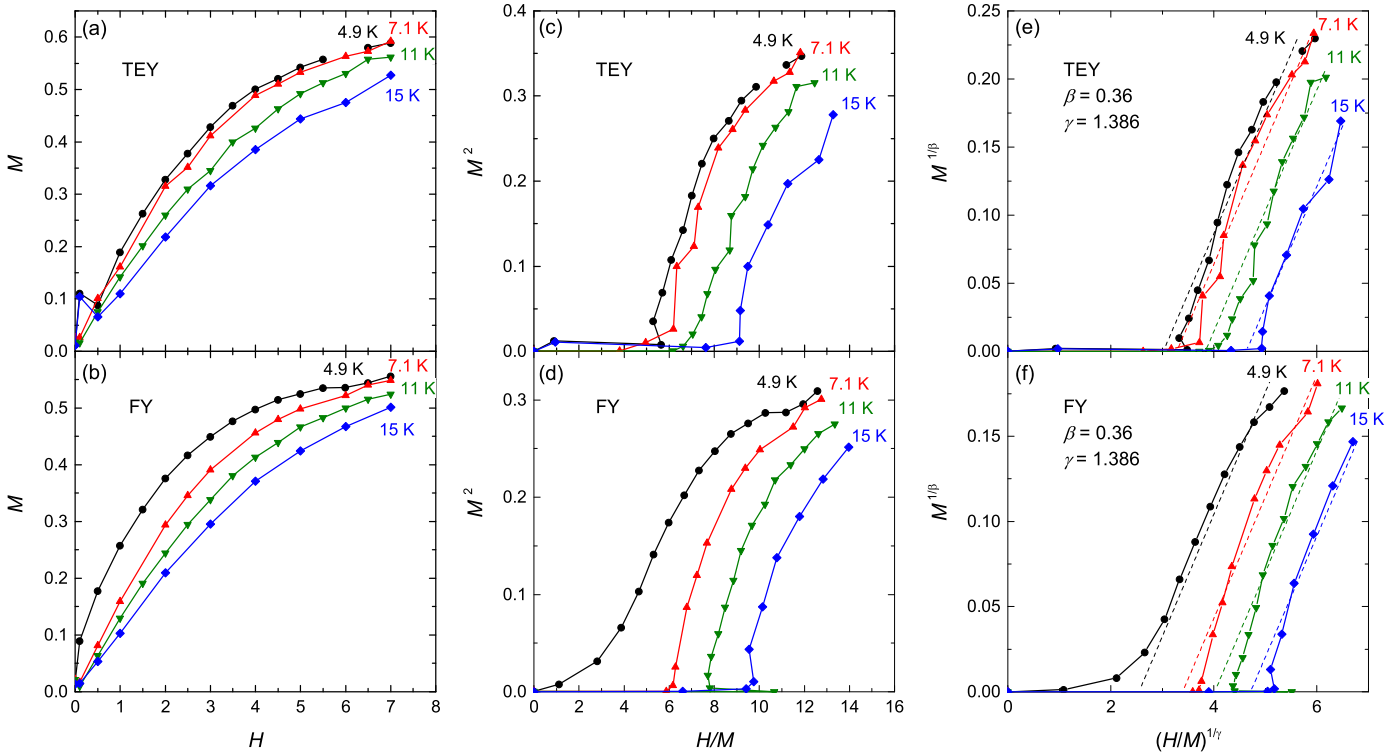

Fig. 3. Magnetization as a function of field, measured by XMCD at various temperatures for the $x=0.113$ sample. Plotted (in arbitrary units) are the isothermal variations of M as a function of H, where H is the applied field and M is the magnetization as determined by the XMCD asymmetry of the Dy M_5 peak. Measurements in TEY detection mode are depicted in the top panels and those in FY in the bottom panels. (a,b) M vs H, (c,d) Arrott plots (i.e., M^2 vs H/M), and (e,f) Arrott–Noakes plots [i.e., M^2 vs $(H/M)^{1/\gamma}$]. For the plots in (e,f), the 3D-Heisenberg model values of $\beta = 0.36$ and $\gamma = 1.386$ were used. Solid lines are guides to the eye only. Dashed lines are linear fits to the high-field region of each isotherm.

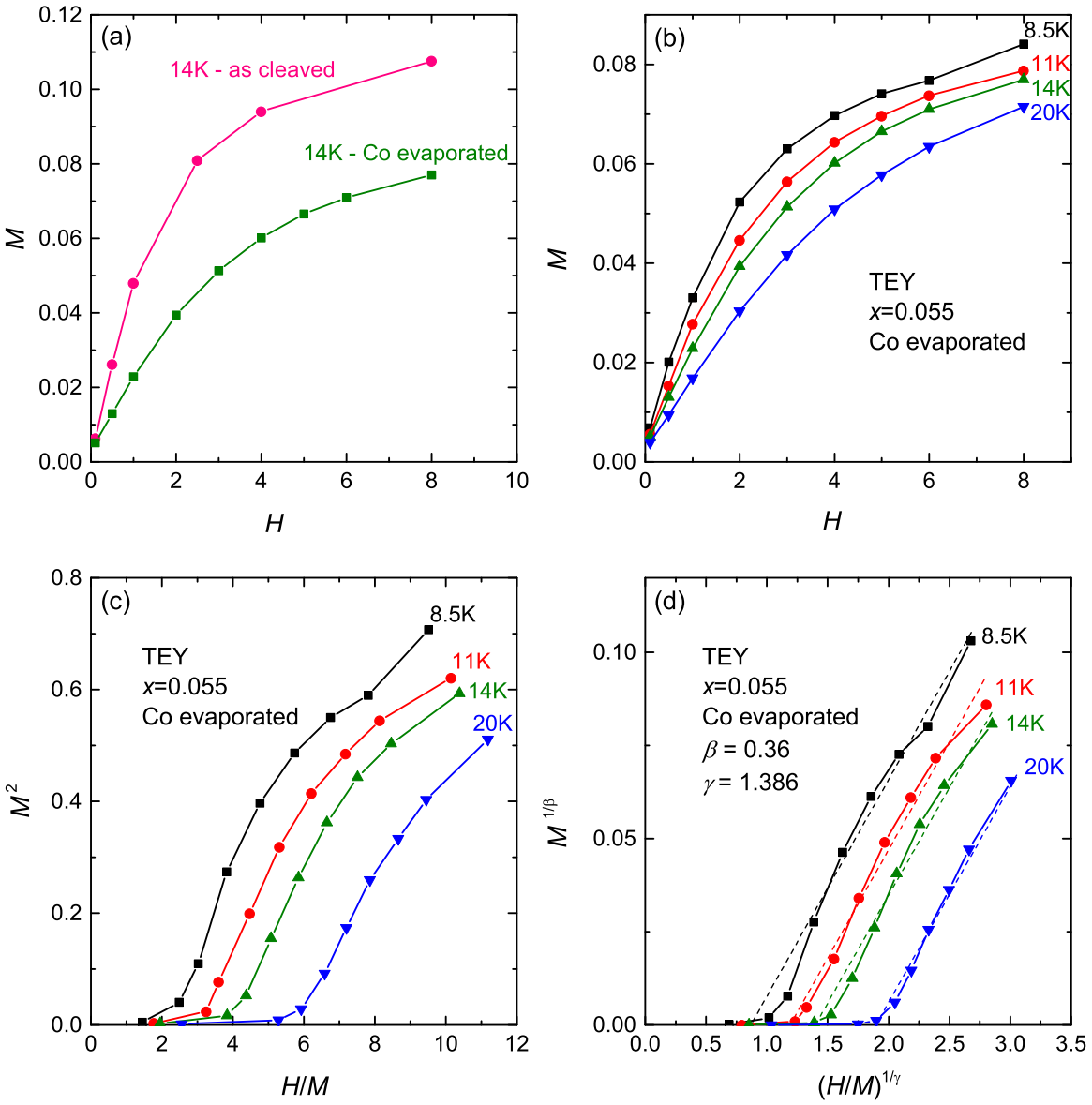

Fig. 4. Magnetization as a function of field, measured by XMCD at various temperatures for the $x=0.055$ sample with Co layer on top. (a) Comparison of M vs H plots measured at 14 K on the as-cleaved surface (pink curve, circles) and after evaporating a thin layer of Co on top (green curve, squares). (b), (c), and (d) show the full set of M vs H, Arrott, and Arrott–Noakes plots, respectively. (For interpretation of the references to color in this figure caption, the reader is referred to the web version of this paper.)

concentrations for the two samples resulting in different magnetic properties [13], only the relative trends can be compared.

These results show that the Co top layer has an adverse effect on the magnetic ordering of the Dy dopants in the Bi_2Te_3 sample in that T_C is decreased. This suggests antiferromagnetic coupling between the Co and Dy atoms at the interface. Even though the Co $L_{2,3}$ XMCD measured in remanence does not indicate antiferromagnetic coupling, one has to bear in mind that, at the temperatures measured, the $(Dy_xBi_{1-x})_2Te_3$ film is paramagnetic so that the exchange interaction between Dy and Co atoms is weak. Furthermore, the remanent field of the superconducting magnet of ~30 mT may be enough to align the Dy and Co atoms.

In RE–transition metal (TM) compounds, the TM 3*d* orbitals are hybridized with the RE 5*d* orbitals with an antiferromagnetic coupling between the spins. In the RE atom, the localized 4*f* electrons couple parallel to the 5*d* spins, so that the resulting indirect 4*f*–3*d* exchange coupling is antiferromagnetic [39]. This has been experimentally confirmed for Dy/Fe and Dy/FeCo amorphous alloys [40] and Dy_xCo_{1-x} compounds [41]. This mechanism also holds for RE–TM interface layers, such as Gd/Fe [42], Gd/CoFe, Tb/NiFe [43], and Dy/CoFe [44]. While magnetically doped TIs do not necessarily behave the same as the aforementioned alloys, compounds, or layer systems, it indicates that an antiferromagnetic coupling is possible.

Clearly, our experimental results show that there is a competition between the magnetic exchange interaction and the Zeeman interaction. The latter favors the Co and Dy magnetic moments to be both aligned in the direction of the applied magnetic field, whereas the atomic exchange interaction is minimized if the Dy and Co atoms are antiferromagnetically aligned, i.e., in zero applied field. However, in order to measure the magnetic moments an applied field is needed to align them. This dilemma is broken by using Arrott plots, where extrapolation to zero field evidences an antiferromagnetic coupling.

5. Summary and conclusions

In summary, we studied the magnetic properties of the surfaces of Dy-doped Bi_2Te_3 in greater detail using surface-sensitive XMCD

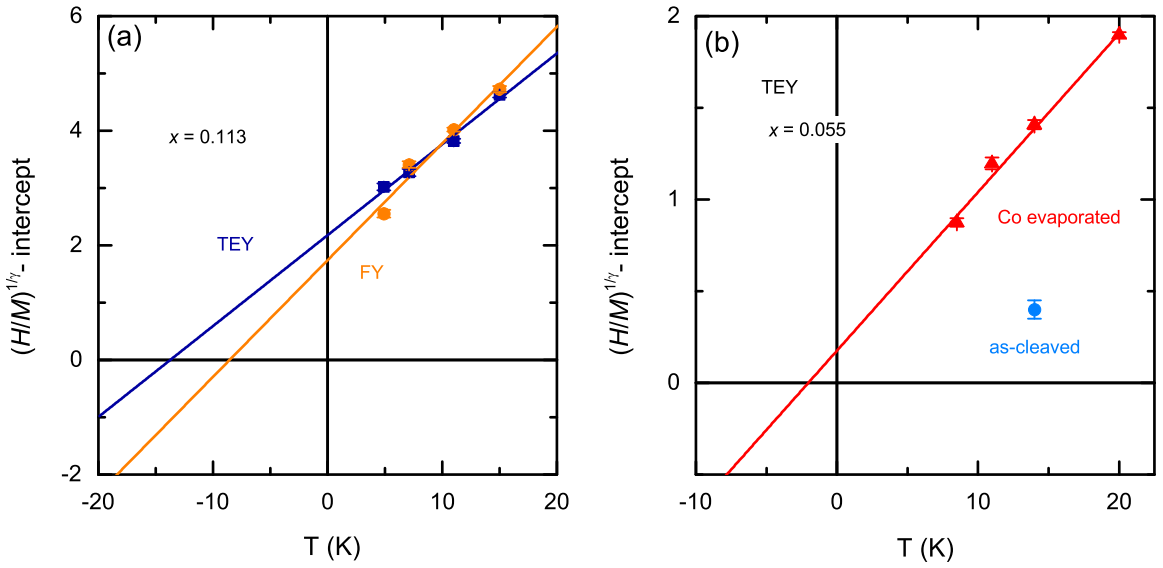

Fig. 5. $(H/M)^{1/\gamma}$ intercepts obtained from the linear fits in Figs. 3 and 4. (a) T_C values extracted for the $x=0.113$ sample are (-14 ± 1) K and (-9 ± 2) K for TEY and FY detection, respectively. (b) T_C obtained from this analysis for the $x=0.055$ sample with the FM Co layer on top is (-2.0 ± 0.8) K.

on *in situ* cleaved thin films. We determined the effective magnetic moment for the $x=0.055$ sample in 7 T field at 6.2 K from multiplet calculation fits to the circularly polarized Dy $M_{4,5}$ spectra to $\sim 5.8\ \mu_B$/Dy. Co adatoms were deposited in an attempt to introduce ferromagnetic long-range order in the films. Using XAS, no change in the chemical state of the Dy atoms was observed as is, in principle, ideal for proximity coupling to the Dy-doped films. The magnetic order on the surfaces was studied in detail using the Arrott–Noakes analysis of the XMCD hysteresis plots as a function of temperature. Using the nearest-neighbor 3D Heisenberg model, the intercepts yield a transition temperature of about -14 K in surface-sensitive TEY mode of the *as-cleaved* film ($x=0.113$). For the $x=0.055$ film, the proximity-coupling to the Co layer gave a lowering of the transition temperature, which suggests an antiferromagnetic ordering scenario. In conclusion we have addressed the outstanding question of ferromagnetism in Dy-doped Bi_2Te_3, finding no evidence of it down to 5 K. This means that another mechanism is responsible for the gap opening seen in these films in ARPES [14]. Our data provides weak indications of an interaction scenario consistent with antiferromagnetic ordering. Recently, it has been reported that antiferromagnetically ordered surfaces could (locally) break TRS, leading to a gap opening [45], which is an interesting concept to explore in the future.

Acknowledgments

Diamond Light Source is acknowledged for beamtime allocated on I10 (SI-10207) and the ESRF for beamtime on ID32 (HC/1282). This publication arises from research funded by the John Fell Oxford University Press (OUP) Research Fund. RCaH is acknowledged for their hospitality. We thank L.J. Collins-McIntyre for help with the MBE growth.

References

[1] Q. Liu, C.-X. Liu, C. Xu, X.-L. Qi, S.-C. Zhang, Magnetic impurities on the surface of a topological insulator, Phys. Rev. Lett. 102 (2009) 156603, http://dx.doi.org/10.1103/PhysRevLett.102.156603.
[2] K. He, Y. Wang, Q.-K. Xue, Quantum anomalous hall effect, Natl. Sci. Rev. 1 (2014) 38, http://dx.doi.org/10.1093/nsr/nwt029.
[3] D.A. Abanin, D.A. Pesin, Ordering of magnetic impurities and tunable electronic properties of topological insulators, Phys. Rev. Lett. 106 (2011) 136802, http://dx.doi.org/10.1103/PhysRevLett.106.136802.
[4] Y.L. Chen, J.-H. Chu, J.G. Analytis, Z.K. Liu, K. Igarashi, H.-H. Kuo, X.L. Qi, S.-K. Mo, R.G. Moore, D.H. Lu, M. Hashimoto, T. Sasagawa, S.C. Zhang, I.R. Fisher, Z. Hussain, Z.X. Shen, Massive Dirac fermion on the surface of a magnetically doped topological insulator, Science 329 (2010) 659–662, http://dx.doi.org/10.1126/science.1189924.
[5] D. Zhang, A. Richardella, D.W. Rench, S.-Y. Xu, A. Kandala, T.C. Flanagan, H. Beidenkopf, A.L. Yeats, B.B. Buckley, P.V. Klimov, D.D. Awschalom, A. Yazdani, P. Schiffer, M.Z. Hasan, N. Samarth, Interplay between ferromagnetism, surface states, and quantum corrections in a magnetically doped topological insulator, Phys. Rev. B 86 (2012) 205127, http://dx.doi.org/10.1103/PhysRevB.86.205127.
[6] M. Watson, L. Collins-McIntyre, A. Coldea, D. Prabhakaran, L.R. Shelford, S. C. Speller, T. Mousavi, C. Grovenor, Z. Salman, S.R. Giblin, G. van der Laan, T. Hesjedal, Study of the structural, electric and magnetic properties of Mn-doped Bi_2Te_3 single crystals, New J. Phys. 15 (2013) 103016, http://dx.doi.org/10.1088/1367-2630/15/10/103016.
[7] P.P.J. Haazen, J.-B. Laloe, T.J. Nummy, H.J.M. Swagten, P. Jarillo-Herrero, D. Heiman, J.S. Moodera, Ferromagnetism in thin-film Cr-doped topological insulator Bi_2Se_3, Appl. Phys. Lett. 100 (2012) 082404, http://dx.doi.org/10.1063/1.3688043.
[8] L.J. Collins-McIntyre, S.E. Harrison, P. Schönherr, N.-J. Steinke, C.J. Kinane, T. R. Charlton, D. Alba-Veneroa, A. Pushp, A.J. Kellock, S.S.P. Parkin, J.S. Harris, S. Langridge, G. van der Laan, T. Hesjedal, Magnetic ordering in Cr-doped Bi_2Se_3 thin films, Europhys. Lett. 107 (2014) 57009, http://dx.doi.org/10.1209/0295-5075/107/57009.
[9] A.I. Figueroa, G. van der Laan, L.J. Collins-McIntyre, S.-L. Zhang, A.A. Baker, S. E. Harrison, P. Schönherr, G. Cibin, T. Hesjedal, Magnetic Cr doping of Bi_2Se_3: evidence for divalent Cr from x-ray spectroscopy, Phys. Rev. B 90 (2014) 134402, http://dx.doi.org/10.1103/PhysRevB.90.134402.
[10] S. Li, S.E. Harrison, Y. Huo, A. Pushp, H.T. Yuan, B. Zhou, A.J. Kellock, S.S. P. Parkin, Y.-L. Chen, T. Hesjedal, J.S. Harris, Magnetic properties of gadolinium substituted Bi_2Te_3 thin films, Appl. Phys. Lett. 102 (2013) 242412, http://dx.doi.org/10.1063/1.4812292.
[11] S.E. Harrison, L.J. Collins-McIntyre, S. Li, A.A. Baker, L.R. Shelford, Y. Huo, A. Pushp, S.S.P. Parkin, J.S. Harris, E. Arenholz, G. van der Laan, T. Hesjedal, Study of Gd-doped Bi_2Te_3 thin films: molecular beam epitaxy growth and magnetic properties, J. Appl. Phys. 115 (2014) 023904, http://dx.doi.org/10.1063/1.4861615.
[12] S.E. Harrison, L.J. Collins-McIntyre, S.L. Zhang, A.A. Baker, A.I. Figueroa, A. J. Kellock, A. Pushp, Y.L. Chen, S.S.P. Parkin, J.S. Harris, G. van der Laan, T. Hesjedal, Study of Ho-doped Bi_2Te_3 topological insulator thin films, Appl. Phys. Lett. 107 (2015) 182406, http://dx.doi.org/10.1063/1.4935235.
[13] S.E. Harrison, L.J. Collins-McIntyre, S.-L. Zhang, A.A. Baker, A.I. Figueroa, A. J. Kellock, A. Pushp, S.S.P. Parkin, J.S. Harris, G. van der Laan, T. Hesjedal, Study of Dy-doped Bi_2Te_3: thin film growth and magnetic properties, J. Phys.: Condens. Matter 27 (2015) 245602, http://dx.doi.org/10.1088/0953-8984/27/24/245602.
[14] S.E. Harrison, L.J. Collins-McIntyre, P. Schönherr, A. Vailionis, V. Srot, P.A. van Aken, A.J. Kellock, A. Pushp, S.S.P. Parkin, J.S. Harris, B. Zhou, Y.L. Chen, T. Hesjedal, Massive Dirac fermion observed in lanthanide-doped topological insulator thin films, Sci. Rep. 5 (2015) 15767, http://dx.doi.org/10.1038/srep15767.
[15] R.R. Biswas, A.V. Balatsky, Impurity-induced states on the surface of three-

dimensional topological insulators, Phys. Rev. B 81 (2010) 233405, http://dx.doi.org/10.1103/PhysRevB.81.233405.
[16] D.K. Efimkin, V. Galitski, Self-consistent theory of ferromagnetism on the surface of a topological insulator, Phys. Rev. B 89 (2014) 115431, http://dx.doi.org/10.1103/PhysRevB.89.115431.
[17] C.-Z. Chang, P. Tang, Y.-L. Wang, X. Feng, K. Li, Z. Zhang, Y. Wang, L.-L. Wang, X. Chen, C. Liu, W. Duan, K. He, X.-C. Ma, Q.-K. Xue, Chemical-potential-dependent gap opening at the Dirac surface states of Bi_2Se_3 induced by aggregated substitutional Cr atoms, Phys. Rev. Lett. 112 (2014) 056801, http://dx.doi.org/10.1103/PhysRevLett.112.056801.
[18] J. Sánchez-Barriga, A. Varykhalov, G. Springholz, H. Steiner, R. Kirchschlager, G. Bauer, O. Caha, E. Schierle, E. Weschke, A.A. Ünal, S. Valencia, M. Dunst, J. Braun, H. Ebert, J. Minár, E. Golias, L.V. Yashina, A. Ney, V. Holý, O. Rader, Nonmagnetic band gap at the Dirac point of the magnetic topological insulator $(Bi_{1-x}Mn_x)_2Se_3$, Nat. Commun. 7 (2016) 10559, http://dx.doi.org/10.1038/ncomms10559.
[19] J.-J. Zhu, D.-X. Yao, S.-C. Zhang, K. Chang, Electrically controllable surface magnetism on the surface of topological insulators, Phys. Rev. Lett. 106 (2011) 097201, http://dx.doi.org/10.1103/PhysRevLett.106.097201.
[20] G. van der Laan, A.I. Figueroa, X-ray magnetic circular dichroism—a versatile tool to study magnetism, Coord. Chem. Rev. 277–278 (2014) 95–129, http://dx.doi.org/10.1016/j.ccr.2014.03.018.
[21] A.A. Baker, A.I. Figueroa, K. Kummer, L.J. Collins-McIntyre, T. Hesjedal, G. van der Laan, Magnetic proximity-enhanced Curie temperature of Cr-doped Bi_2Se_3 thin films, Phys. Rev. B 92 (2015) 094420, http://dx.doi.org/10.1103/PhysRevB.92.094420.
[22] B.T. Thole, G. van der Laan, J.C. Fuggle, G.A. Sawatzky, R.C. Karnatak, J.-M. Esteva, 3*d* x-ray-absorption lines and the $3d^9 4f^{n+1}$ multiplets of the lanthanides, Phys. Rev. B 32 (1985) 5107, http://dx.doi.org/10.1103/PhysRevB.32.5107.
[23] M. van Veenendaal, R. Benoist, X-ray absorption and resonant inelastic x-ray scattering in the rare earths, Phys. Rev. B 58 (1998) 3741–3749, http://dx.doi.org/10.1103/PhysRevB.58.3741.
[24] L.R. Shelford, T. Hesjedal, L. Collins-McIntyre, S.S. Dhesi, F. Maccherozzi, G. van der Laan, Electronic structure of Fe and Co magnetic adatoms on Bi_2Te_3 surfaces, Phys. Rev. B 86 (2012) 081304(R), http://dx.doi.org/10.1103/PhysRevB.86.081304.
[25] G. van der Laan, Hitchhiker's guide to multiplet calculations, Lect. Notes Phys. 697 (2006) 143–199, http://dx.doi.org/10.1007/b11594864.
[26] R.D. Cowan, The Theory of Atomic Structure and Spectra, University of California Press, Berkeley, 1981.
[27] G. van der Laan, B.T. Thole, Strong magnetic x-ray dichroism in 2*p* absorption spectra of 3*d* transition-metal ions, Phys. Rev. B 43 (1991) 13401–13411, http://dx.doi.org/10.1103/PhysRevB.43.13401.
[28] B.T. Thole, P. Carra, F. Sette, G. van der Laan, X-ray circular dichroism as a probe of orbital magnetization, Phys. Rev. Lett. 68 (1992) 1943–1946, http://dx.doi.org/10.1103/PhysRevLett.68.1943.
[29] P. Carra, B.T. Thole, M. Altarelli, X. Wang, X-ray circular dichroism and local magnetic fields, Phys. Rev. Lett. 70 (1993) 694–697, http://dx.doi.org/10.1103/PhysRevLett.70.694.
[30] G. van der Laan, Sum rule practise, J. Synchrotron Rad. 6 (1999) 694–695, http://dx.doi.org/10.1107/S0909049599000412.
[31] G. van der Laan, E. Arenholz, A. Schmehl, D.G. Schlom, Weak anisotropic x-ray magnetic linear dichroism at the $M_{4,5}$ edges of ferromagnetic EuO(001): evidence for 4*f*-state contributions, Phys. Rev. Lett. 100 (2008) 067403, http://dx.doi.org/10.1103/PhysRevLett.100.067403.
[32] J.B. Goedkoop, B.T. Thole, G. van der Laan, G.A. Sawatzky, F.M.F. de Groot, J. C. Fuggle, Calculations of magnetic x-ray dichroism in the 3*d* absorption spectra of rare earth compounds, Phys. Rev. B 37 (1988) 2086–2095, http://dx.doi.org/10.1103/PhysRevB.37.2086.
[33] A. Agui, M. Mizumaki, T. Asahi, K. Matsumoto, T. Morikawa, J. Sayama, T. Osaka, Microscopic magnetic property of perpendicular magnetic films of Dy_xCo_{100-x} measured using soft x-ray magnetic circular dichroism, J. Phys. Chem. Solids 68 (2007) 2148, http://dx.doi.org/10.1016/j.jpcs.2007.08.041.
[34] R. Westerström, J. Dreiser, C. Piamonteze, M. Muntwiler, S. Weyeneth, H. Brune, S. Puponi, F. Nolting, A. Popov, S. Yang, L. Dunsch, T. Greber, An endohedral single-molecule magnet with long relaxation times: $DySc_2N@C_{80}$, J. Am. Chem. Soc. 134 (2012) 9840–9843, http://dx.doi.org/10.1021/ja301044p.
[35] R. Westerström, A.-C. Uldry, R. Stania, J. Dreiser, C. Piamonteze, M. Muntwiler, F. Matsui, S. Rusponi, H. Brune, S. Yang, A. Popov, B. Büchner, B. Delley, T. Greber, Surface aligned magnetic moments and hysteresis of an endohedral single-molecule magnet on a metal, Phys. Rev. Lett. 114 (2015) 087201, http://dx.doi.org/10.1103/PhysRevLett.114.087201.
[36] B.G. Wybourne, L. Smentek, Optical Spectroscopy of Lanthanides. Magnetic and Hyperfine Interaction, CRC Press, Boca Raton, Florida, 2007.
[37] A. Arrott, Criterion for ferromagnetism from observations of magnetic isotherms, Phys. Rev. 108 (1957) 1394–1396, http://dx.doi.org/10.1103/PhysRev.108.1394.
[38] A. Arrott, J.E. Noakes, Approximate equation of state for nickel near its critical temperature, Phys. Rev. Lett. 19 (1967) 786–789, http://dx.doi.org/10.1103/PhysRevLett.19.786.
[39] M.S.S. Brooks, L. Nordstrom, B. Johansson, Origin and ab initio evaluation of magnetic interactions in rare earth intermetallics, J. Phys.: Condens. Matter 3 (1991) 3393–3396, http://dx.doi.org/10.1088/0953-8984/3/19/018.
[40] K. Fleury-Frenette, S.S. Dhesi, G. van der Laan, D. Strivay, G. Weber, J. Delwiche, Characteristics of the iron moment in Dy-Fe and Dy-FeCo amorphous alloys studied by x-ray magnetic circular dichroism, J. Magn. Magn. Mater. 220 (2000) 45–51, http://dx.doi.org/10.1016/S0304-8853(00)00460-1.
[41] K. Chen, D. Lott, F. Radu, F. Choueikani, E. Otero, P. Ohresser, Observation of an atomic exchange bias effect in $DyCo_4$ film, Sci. Rep. 5 (2015) 18377, http://dx.doi.org/10.1038/srep18377.
[42] D. Haskel, G. Srajer, J.C. Lang, J. Pollmann, C.S. Nelson, J.S. Jiang, S.D. Bader, Enhanced interfacial magnetic coupling of Gd/Fe multilayers, Phys. Rev. Lett. 87 (2001) 207201, http://dx.doi.org/10.1103/PhysRevLett.87.207201.
[43] W. Zhang, D. Zhang, P.K.J. Wong, H. Yuan, S. Jiang, G. van der Laan, Y. Zhai, Z. Lu, Selective tuning of gilbert damping in spin-valve trilayer by insertion of rare-earth nanolayers, ACS Appl. Mater. Interfaces 7 (2015) 17070–17075, http://dx.doi.org/10.1021/acsami.5b03595.
[44] M.K. Marcham, W. Yu, P.S. Keatley, L.R. Shelford, P. Shafer, S.A. Cavill, H. Qing, A. Neudert, J.R. Childress, J.A. Katine, E. Arenholz, N.D. Telling, G. van der Laan, R.J. Hicken, Influence of a Dy overlayer on the precessional dynamics of a ferromagnetic thin film, Appl. Phys. Lett. 102 (2013) 062418, http://dx.doi.org/10.1063/1.4792740.
[45] L. Oroszlany, A. Cortijo, Gap generation in topological insulator surface states by nonferromagnetic magnets, Phys. Rev. B 86 (2012) 195427, http://dx.doi.org/10.1103/PhysRevB.86.195427.